Structural controls and relative timing of gold mineralization of the banded iron formation-associated Tiriganiaq deposit, Meliadine district, Rankin Inlet greenstone belt, Nunavut

Brayden St.Pierre[1], Patrick Mercier-Langevin[2], Jean-Claude Blais[3], Guilhem Servelle[3], Marjorie Simard[4], Olivier Côté-Mantha[5], and Michel Malo[1]

[1]Institut national de la Recherche scientifique, Centre Eau Terre Environnement, 490 rue de la Couronne, Québec, Quebec G1K 9A9
[2]Geological Survey of Canada, 490 rue de la Couronne, Québec, Quebec G1K 9A9
[3]Agnico Eagle Mines Limited, Meliadine Division, Rankin Inlet, Nunavut X0C 0G0
[4]Agnico Eagle Mines Limited, Technical Services, 200 route de Preissac, Rouyn Noranda, Quebec J0Y 1C0
[5]Agnico Eagle Mines Limited, Exploration Division, 765 chemin de la mine Goldex, Val-d'Or, Quebec J9P 7G4
*Corresponding author's e-mail: braydenstpierre.geo@gmail.com

ABSTRACT

The Meliadine gold district is hosted within the Archean (ca. 2660 Ma) polydeformed Rankin Inlet greenstone belt, Nunavut. The district comprises numerous gold deposits and prospects that are spatially associated with the Pyke Fault and its splays. This includes the currently producing Tiriganiaq deposit, which is hosted within the turbidite-dominated structural hanging wall of the Lower Fault, a west-trending splay of the Pyke Fault.

The 1150 and 1250 "lode series" within the Tiriganiaq deposit are a series of ore zones with complex geometries. Before underground development, the knowledge of gold-grade distribution in these zones was based on surface drilling results and could therefore not take into account some of the small-scale structural features that control ore grade and ore zone geometry (e.g. <25 m wavelength folding).

New field relationships document the importance of horizontal to shallowly south-dipping ore-bearing extensional quartz±ankerite veins. These veins are associated with sulphide replacement zones that are preferentially developed in tightly folded banded iron formation (BIF) intervals. Folding and veining are associated with the main phase of deformation in the deposit area, which corresponds to the second phase (D_2) of regional deformation. The D_2 deformation at the Tiriganiaq deposit can be further subdivided into two main protracted phases: the first phase (D_2A), which is associated with northeast-southwest-oriented shortening and F_2A folding; and the second phase (D_2B), which is associated with north-south shortening, further folding (F_2B), and reverse shearing and veining (shallowly south-dipping extension veins and moderately north-dipping shear veins). The 1150 and 1250 lodes provide an excellent example of the complex geometry of the ore-bearing veins found within the shallowly west-plunging F_2B folded BIF successions. These zones provide some of the highest gold grades within the Tiriganiaq deposit and thus highlight the importance of fold hinges and their effect on the generation of favourable traps (thickened BIF intervals), the development of narrow shears (along the limbs), and the development of associated extensional veins in the competent BIF layers, forming structurally and lithologically controlled high-grade zones.

INTRODUCTION

Banded iron formation (BIF) represents an important host rock for a large number of world-class gold deposits, including the archetypical BIF-hosted Homestake mine, South Dakota, USA, which produced 40 million ounces (>1240 t) of gold (Bell, 2013). Other large BIF-hosted gold deposits include the Morro Velho mine in Minas Gerais, Brazil, which has produced over 15 million ounces (>465 t) of gold in almost 300 years of production (Vial et al., 2007) as well as past or currently producing Canadian mines such as Hardrock, Musselwhite, and Pickle Crow in Ontario and Lupin in Nunavut. The exceptional gold endowment of these deposits is due, at least in part, to the Fe-rich nature of the host rocks. Experimental geochemistry suggests that the solubility of gold within moderate-temperature hydrothermal fluids is favoured by S-ligands. These S-Au complexes are destabilized during fluid:rock interaction with Fe-rich rocks (Phillips et al., 1984), which is reflected in the rock record by the ubiquitous association between gold and sulphide-replacement zones (e.g. arsenopyrite, pyrite, and pyrrhotite) at most BIF-hosted deposits.

St.Pierre, B., Mercier-Langevin, P., Blais, J.-C., Servelle, G., Simard, M., Côté-Mantha, O., and Malo, M., 2020. Structural controls and relative timing of gold mineralization of the banded iron formation-associated Tiriganiaq deposit, Meliadine district, Rankin Inlet greenstone belt, Nunavut; *in* Targeted Geoscience Initiative 5: Contributions to the Understanding of Canadian Gold Systems, (ed.) P. Mercier-Langevin, C.J.M. Lawley, and S. Castonguay; Geological Survey of Canada, Open File 8712, p. 237–250. https://doi.org/10.4095/326041

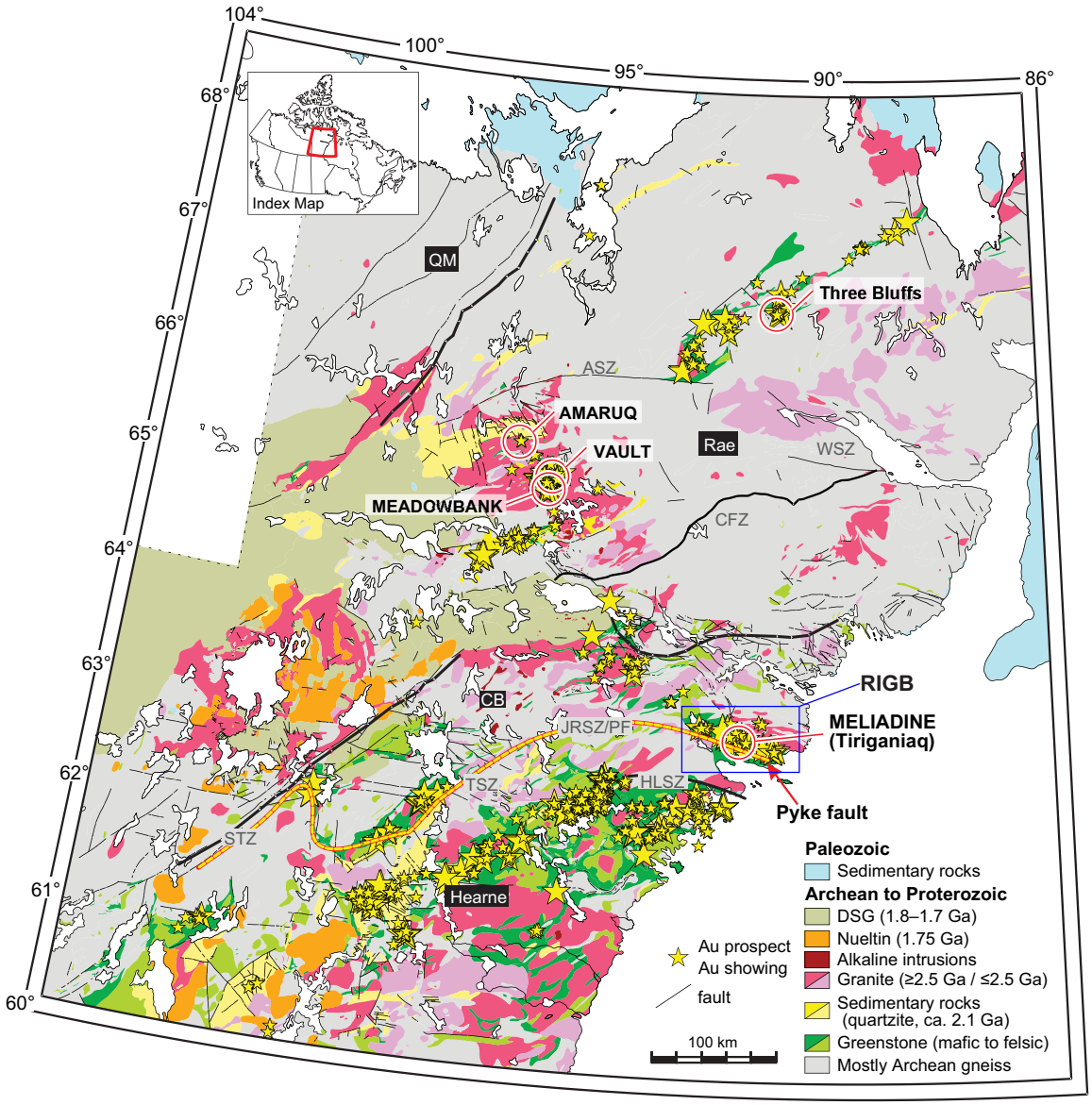

Figure 1. Western Churchill Province regional geology map showing the location of the Rankin Inlet greenstone belt (RIGB) and Meliadine gold district (MGD) and the distribution of other gold deposits, prospects, and showings of the region. Abbreviations: ASZ = Amer shear zone, CB = Chesterfield block, CFZ = Chesterfield Fault zone, DSG = Dubawant Super Group, HLSZ = Happy Lake shear zone, JRSZ = Josephine River shear zone, PF = Pyke Fault, QM = Queen Maud block, STZ = Snowbird Tectonic Zone, TSZ = Tyrrell shear zone, NWT = Northwest Territories, WSZ = Wager shear zone. *Modified from* Lawley et al. (2016).

Many of the so-called BIF-hosted gold deposits in the Western Churchill Province, including Meadowbank, Amuruq, and Tiriganiaq, are only partially BIF-hosted (i.e. BIF-associated: cf. Dubé et al., 2015). These major gold districts provide compelling evidence that a variety of depositional mechanisms control the distribution of gold, including structural and rheological lithological factors. Structural controls are commonly reflected in the close spatial relationship between gold ore zones and complexly deformed rocks at all scales, i.e., ranging from the distribution of the deposits to the internal textures and structures of the ore (Robert et al., 1994; Goldfarb et al., 2005). Layer anisotropy and/or competency contrasts between BIFs and the surrounding sedimentary or volcanic rocks create favourable structural and chemical traps for auriferous fluids, as suggested by the variety of ore-bearing vein styles at many deposits (Dubé et al., 2015 and references therein). However, the complete structural history and its controls on gold mineralization often remain equivocal at most BIF-hosted and BIF-associated gold deposits due to complex brittle-ductile fault-zone behaviour and/or multiple generations of folding and faulting.

The Meliadine gold district (MGD), located within the ca. 2660 Ma Rankin Inlet greenstone belt (RIGB), Nunavut (Fig. 1), is one of Canada's largest emerging

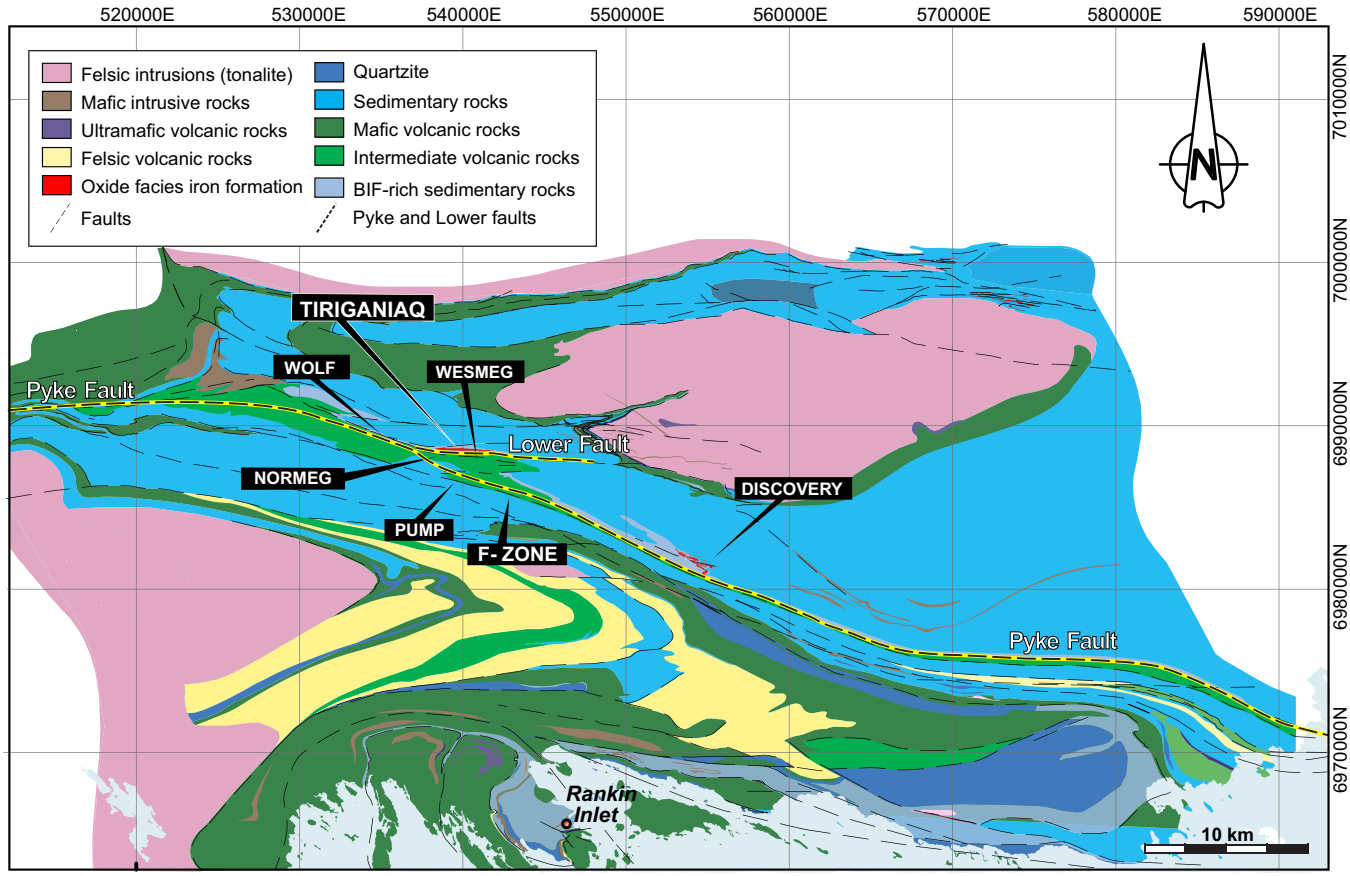

Figure 2. Geological map of the Meliadine gold district showing the location of the Tiriganiaq and other gold deposits and major prospects within the area. The alignment of gold deposits and occurrences in the district is defined by the northwest-trending major Pyke Fault zone. *Compiled from* Agnico Eagle Mines Limited (unpub. internal reports) and Comaplex Minerals Corporation legacy material (e.g. Barham, 2010 and references therein). Abbreviation: BIF = banded iron formation.

BIF-associated gold districts with 3.7 million ounces (115.1 t) of gold in proven and probable reserves, 3.1 million ounces (96.4 t) of gold in indicated resources, and 2.7 million ounces (84 t) of gold in inferred resources as of December 31, 2018 (Agnico Eagle Mines Limited, 2019). The MGD comprises numerous orogenic gold deposits and prospects that are spatially associated with the Pyke Fault and its splays (Fig. 2). Many of these gold deposits are BIF-associated, including Tiriganiaq, the largest deposit of the district. The Tiriganiaq deposit (Meliadine mine) entered into production in mid-May 2019 and is expected to produce 230,000 ounces (7.2 t) of gold in 2019 (including pre-commercial production), and 385,000 ounces (12 t) in 2020, its first full year of production (Agnico Eagle Mines Limited, 2019).

The timing of gold mineralization at the Tiriganiaq deposit and, more broadly across the Western Churchill Province, has yet to be precisely established. The uncertainty of the timing of the gold is due largely to the lack of bedrock exposure, the short timeframe of exploration and academic assessment relative to other major mining districts in Canada, and a protracted history of deformation and resultant geometric complexity. Nevertheless, the broad timing of gold introduction has been attributed to reworking and metamorphism during the Trans-Hudson Orogeny (1.9–1.8 Ga; Carpenter and Duke, 2004; Carpenter et al., 2005; Lawley et al., 2015a,b,c, 2016).

Exploration and previous research in the area in the last few decades led to a first-order understanding of the main ore zones at the Tiriganiaq deposit (e.g. Carpenter and Duke, 2004; Carpenter et al., 2005; Lawley et al., 2015a,b,c, 2016). The model was however challenged when underground development started of the 1150 and 1250 “lode series”, which highlighted structural complexities within the multiply folded BIF units. These multiply deformed ore horizons are challenging to model in 3-D, which impacts mine production and grade and tonnage estimations. Active mining has provided access to underground exposures of the 1150 and 1250 lode series. Detailed geological and structural mapping was carried out along newly developed drifts that exposed the footwall and extended beyond the 1150 lode series into the structural hanging wall.

This report summarizes the current status of the ongoing multidisciplinary research being conducted at

the Meliadine mine. In part, this project aims to constrain the structural and lithological controls on the formation and distribution of the BIF-hosted gold mineralization in the 1150 and 1250 lode series at the Tiriganiaq deposit. Most of the new results are based on underground drill-core observations, but also included are sampling for structural, petrographic, and geochemical analyses. This study builds on previous research in the MGD (e.g. Carpenter and Duke, 2004; Carpenter et al., 2005; Lawley et al., 2015a,b, 2016) to expand knowledge on the structural history and the relative timing of events in a complexly folded and sheared gold-rich BIF-associated ore zones. These new results provide a robust structural and geological framework for mineralization within the 1150 and 1250 ore zones and have led to a more precise geological model, stope design, and resource estimation.

REGIONAL GEOLOGICAL SETTING

The RIGB is located within the Western Churchill Province along the southern margin of the Chesterfield Block, near the boundary with the Hearne Craton (Fig. 1; Berman et al., 2007; Pehrsson et al., 2013; Lawley et al., 2015a,b,c, 2016). This boundary between the Chesterfield Block and the Hearne Craton is inferred to represent a crustal-scale feature but it is obscured by ca. 1800 Ma plutonism, multiple deformation stages, and by the lack of bedrock exposure. At surface it likely forms a broad, structurally imbricated zone rather than a discrete lineament (Lawley et al., 2015b) and may include part of the Tyrrell shear zone (MacLachlan et al., 2005) and/or Happy Lake shear zone (Fig. 1; Berman et al., 2002).

The RIGB is a polydeformed and metamorphosed sequence of intercalated ca. 2660 Ma mafic volcanic and turbiditic successions deposited on an unexposed Meso- to Neoarchean substrate (Lawley et al., 2016). Neoarchean rocks are intruded by undeformed and metamorphosed ≤1830 Ma lamprophyre dykes (Fig. 2; Tella, 1994; Carpenter and Duke, 2004; Carpenter et al., 2005; Lawley et al., 2015a,b,c, 2016). The RIGB has been subdivided into two volcanic cycles (Tella et al., 1986) or assemblages (Bannatyne, 1958): 1) Lower Volcanic Assemblage (LVA), and 2) Upper Volcanic Assemblage (UVA). Abundant mafic to ultramafic dykes and sills of unknown age crosscut the UVA and LVA (Lawley et al., 2015a,b,c, 2016).

The RIGB is interpreted as an east-dipping homocline that has been folded into a southeast-plunging upright F_2 synform (Tella et al., 1986; Tella, 1994; Carpenter and Duke, 2004; Carpenter et al., 2005). The MGD consists of multiple gold deposits and prospects that are spatially associated with the west- to west-northwest-trending and steeply north-dipping Pyke Fault and its subsidiary splays (Fig. 2; Tella et al., 1992, 1996; Carpenter and Duke, 2004). Carpenter and Duke (2004) have separated the deformation history of the RIGB into four increments. The oldest phase of deformation (D_1) lacks identifiable cleavage, but likely represents the initial juxtaposition of turbiditic and volcanic rock packages along an ancestral expression of what most probably now forms the Pyke Fault (Carpenter and Duke, 2004; Carpenter et al., 2005; Lawley et al., 2015a,b,c, 2016). This early phase of deformation has been inferred to explain the close intercalation of geochemically distinct mafic volcanic rocks (Lawley et al., 2016). The second phase of deformation (D_2) consisted of folding of the Archean successions by northeast-southwest shortening, which resulted in F_2 folds and an axial-planar S_2 cleavage. The third phase of deformation (D_3) consisted of a slight change of direction from northeast-southwest-directed to north-south-directed shortening (Carpenter and Duke, 2004), forming a west-trending fabric. At the Tiriganiaq deposit, there is one dominant fabric oriented at approximately N265/65, which has been interpreted by Miller et al. (1995) to represent the main regional S_2 foliation that was transposed into a west-trending orientation during D_3 deformation. The fourth deformation (D_4) fabrics consist of small-scale kink bands and a locally well developed north- to northwest-trending crenulation cleavage (Carpenter and Duke, 2004; Carpenter et al., 2005).

Deposit Stratigraphy

The Tiriganiaq deposit, located in the central part of the Meliadine district, is hosted in the overturned and dominantly turbidite-hosted structural hanging wall of the Lower Fault. The structural hanging wall comprises three distinct sedimentary formations stacked from south to north (Fig. 2–4): 1) the mineralized Tiriganiaq Formation, a package of laminated siltstone with graphitic argillite at its base, in contact with the Lower Fault; 2) the Upper Oxide Formation, a diverse package of iron-rich turbidite layers intercalated with complexly folded silicate-facies and oxide-facies BIF units, which host the majority of the ore at Tiriganiaq, including the 1150 and 1250 lode series (Fig. 3); and 3) the northern-most formation, the Sam Formation, which is a stacked package of laminated siltstone and greywacke.

South of the Lower Fault (i.e. structural footwall) the Wesmeg Formation comprises mafic volcanic rocks intercalated with interflow sedimentary rocks and oxide-facies BIF units. These rocks are cut by gabbro and lamprophyre dykes. The Normeg, Wesmeg, F-zone, and Pump orebodies are all hosted in the Wesmeg Formation (Fig. 2, 3).

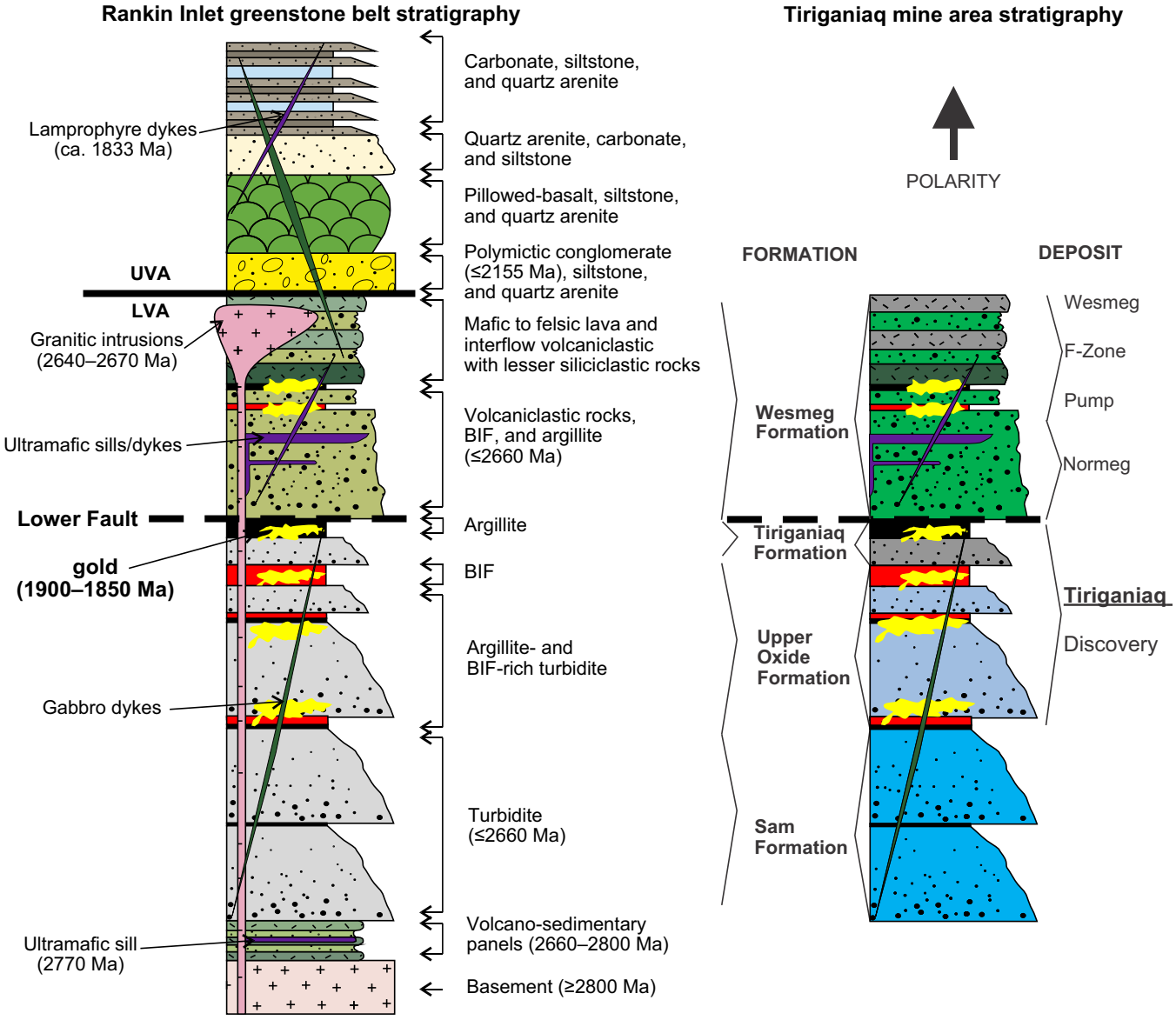

Figure 3. Lithostratigraphic columns of the Rankin Inlet greenstone belt (*modified from* Lawley et al., 2016) and the Tiriganiaq deposit area, displaying relative ages of the lithologies and the crosscutting relationships. The Tiriganiaq deposit area stratigraphic column colour scheme coincides with other diagrams in this contribution. Abbreviation: BIF = banded iron formation, LVA = Lower Volcanic Assemblage, UVA = Upper Volcanic Assemblage.

METHODOLOGY

Detailed underground geological and structural mapping was carried out in 2017 and 2018 along newly developed drifts that exposed the footwall and extended beyond the 1150 lode series into the structural hanging wall. Lithology, alteration, and structural measurements were recorded on georeferenced base maps of drift walls and backs that were surveyed by the Meliadine mine engineering team. Systematic logging and sampling of drill core were completed on a set of representative sections to link observations made from mapping with petrographic and whole-rock lithogeochemistry. Detailed underground mapping and observations are the focus of this contribution.

RESULTS

Structure

At the deposit scale, and based on the observations made in this study, the structural history can be subdivided into three deformation events (Table 1). The earliest deformation event (D_1) at Tiriganiaq, which is inferred from regional-scale observations, has resulted in sedimentary units being thrust on top of volcanic units by the north-dipping Lower Fault. The second deformation event (D_2) can be separated into three phases based on detailed underground observations of bedding, foliation, shear-plane development, and crosscutting relationships. The first phase of the second deformation event (D_2A) (D_2 deformation in Carpenter

Table 1. Summary table of the relative timing of events, including interpreted timing, cause, and characteristics of mineralization.

Age	Event	Description	Associated Structures	Associated Veins and Characteristics	Mineralization
Archean ?	**D_1?**	**D_1**- Initial juxtaposition of mafic volcanic package on top of turbiditic sequence	Ancestral north-verging thrust? S_0/S_1	Quartz along proto Pyke Fault/Lower Fault?	?
Paleoproterozoic (1.90–1.83 Ga)	**D_2**	**D_2A** - Onset of NE-SW shortening resulting in layer parallel folding	**S_2A** - Regional penetrative fabric **F_2A** - Isoclinal folds	Onset of main quartz-ankerite 1000 lode shear vein along Lower Fault	Arsenopyrite+gold precipitation in main shear within 1000 lode and septae
		D_2B - Progressive N-S shortening characterized by mixed brittle and ductile deformation	**S_2B** - Local EW cleavage development axial planar to regional asymmetric **F_2B** - Z-folds Shear plane development oblique to and dragging S_2A foliation indicating north over south motion within 1150 and 1250 lodes	Onset of quartz-ankerite shear veins and associated extensional veins within the 1150 and 1250 lode series Onset of extensional vein arrays north of the 1000 lode	Arsenopyrite+gold precipitation in main shear within 1000 lode and septae Stratabound arsenopyrite+gold along extensional vein selvages within BIF packages
		D_2C - Final stage of N-S shortening and associated reverse shearing, moving towards a more brittle regime	**S_2C** - N-NW crenulation cleavage and kink bands overprinting S_2A and S_2B	Some continuation of veining with same sigma orientation to D_2B Progressive deformation of extension vein arrays Continuation of 1000 lode formation	Arsenopyrite+gold within 1000 lode and septae Further gold mineralization within shear zones and associated extension

and Duke, 2004 and Carpenter et al., 2005; D_2A deformation in Miller et al., 1995) involved layer-parallel F_2A isoclinal folding of the host succession (e.g. Fig. 4) and the associated development of axial-planar, regionally penetrative S_2A cleavage, as well as reverse displacements along the Pyke and Lower faults. The second phase of the second deformation event (D_2B) (D_3 in Carpenter and Duke, 2004 and Carpenter et al., 2005; D_2B in Miller et al., 1995) marks a slight change of shortening orientation to north-south, creating west-trending regional F_2B asymmetric Z-folds (transposed F_2A folds at ore-zone scale) and a west-trending, moderately north-dipping (~45–70º) axial-planar S_2B cleavage that overprints the S_2A foliation. The S_2A foliation is commonly re-oriented into the S_2B fabric in narrow D_2B high-strain zones, forming a composite foliation. The S_2B shear fabric has a slightly shallower dip than the S_2A foliation and dragging of the west-trending S_2A foliation into the D_2B shears indicates a reverse (north-over-south) motion within west-trending decimetre- to metre-wide shear zones localized within chloritic-siltstone units intercalated within decimetre- to metre-wide F_2B folded BIF. The third phase of the second deformation event (D_2C) (D_4 in Carpenter and Duke 2004 and Carpenter et al., 2005; D_3 in Miller et al., 1995) consists of a S_2C crenulation cleavage and associated kink bands.

The D_3 deformation is characterized by box folds within well foliated rocks along the Lower Fault zone. Brittle fault gouges that overprint previous fabrics/structures (Fig. 5a) likely represent a phase of relaxation in a brittle regime immediately after major reverse motion (*see* Discussion *below*).

Mineralization and Structural Style

Tiriganiaq is a BIF-associated gold deposit (Dubé et al., 2015; Lawley et al., 2015a). At Tiriganiaq, gold mineralization largely consists of decimetre to metre thick laminated fault-fill and associated extensional veins with coarse arsenopyrite and minor pyrrhotite replacement of magnetite-rich layers in BIF units along vein selvages. Gold is paragenetically late and, at the micro-scale, occurs within low-strain micro-textural sites and clusters of inclusions within variably recrystallized and idioblastic arsenopyrite crystals (Carpenter et al., 2005; Lawley et al., 2015a,b,c, 2016).

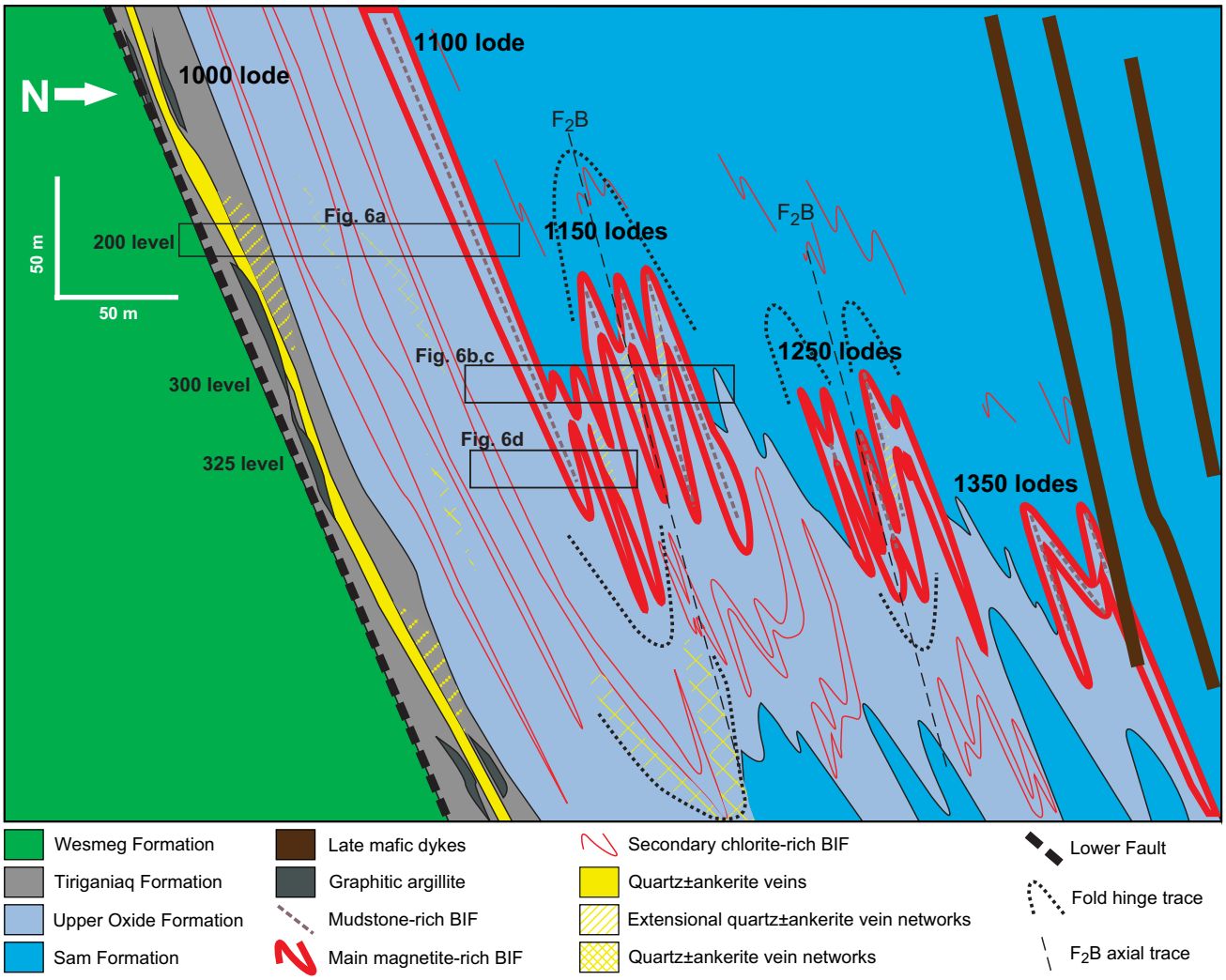

Figure 4. Schematic section of the Tiriganiaq deposit and its various ore zones (or "lodes"), looking west. The section shows the geometry of the different volcano-sedimentary formations, vein distribution, and the ore zone locations (*modified from* Agnico Eagles Mines Limited, unpubl. internal reports). Abbreviation: BIF = banded iron formation.

The 1000 lode vein (Fig. 4), hosted in the Tiriganiaq Formation, is a quartz±ankerite laminated shear vein (Fig. 5b,c) spatially associated with the Lower Fault. The syn-D_2 deformation 1000 lode vein is planar, but pinches and swells vertically and laterally and has an alteration halo comprising sericite±ankerite and coarse euhedral arsenopyrite, pyrrhotite, and minor galena (Lawley et al., 2015c). Sections of the 1000 lode that contain abundant deformed, horizontal to shallowly north-dipping, syn- to late-D_2B quartz±ankerite±gold extensional vein arrays (Fig. 5c) are part of a zone that is referred to as the "intervening lodes", which is located between the 1000 lode and the 1100 lode. These areas of intense veining contain significant concentrations of gold and are thus areas of great interest and the subject of an ongoing M.Sc. thesis at Université du Québec à Montréal, which aims to further the understanding of the controls on their development and to determine if they define ore shoots at the deposit scale.

Approximately 75–80% of the ore at the Tiriganiaq deposit is hosted within the Upper Oxide Formation, including the 1100 lode, which is associated with the transposed long limb of a F_2B fold that affects the BIF succession (Fig. 4, 6a). Gold mineralization comprises contact-parallel shear veins and horizontal to shallowly south-dipping quartz-ankerite extension veins that are preferentially developed in BIF units. Coarse arsenopyrite and minor pyrrhotite replacement of magnetite-rich layers in BIF units often occur along the selvages of these veins (Fig. 5d–g, 6b–d).

Detailed Underground Mapping of the 1150 and 1250 Lode Series

Figure 5 illustrates the main lithological and structural relationships observed in mapping the 1150 and 1250 lode series. In Figure 5d, D_2B mineralized reverse shear zones localized within chloritic siltstone contain mineralized quartz±ankerite veins along S_2B shear

planes that drag the S_2A foliation. Horizontal to shallowly south-dipping mineralized extensional veins, associated with the mineralized D_2B reverse shear zones, preferentially form within intercalated decimetre to metre wide F_2B-folded BIF (Fig. 5e-f). These horizontal to shallowly south-dipping extensional veins typically have coarse arsenopyrite and minor pyrrhotite replacement of magnetite-rich layers in BIF units occurring along the selvages of these veins (Fig. 5e-g). Figure 6 presents four detailed maps of underground exposures of the 1000, 1100, and 1150 lodes. These maps provide details about the host units, structural style, and distribution of the mineralized zones. The Upper Oxide Formation hosts the geometrically and structurally complex 1150 and 1250 lode series, which are controlled by narrow, syn- to late-D_2B deformation, Lower Fault-parallel and north-dipping reverse shear zones, which overprint the slightly steeper, north-dipping S_2A foliation (Fig. 5d, 6b–d). The earlier S_2A foliation is axial planar to tight F_2A folds (Fig. 4, 6).

Draw-point DP200-161

Draw-point DP200-161 (Fig. 6a) preserves the planar nature of the Lower Fault, the 1000 lode, and the 1100 lode. The Lower Fault is slightly less steep than the surrounding dominant S_2A fabric. The 1000 lode is defined by planar, laminated, composite quartz±ankerite shear veins spatially associated with Lower Fault. The 1100 lode, or ore zone, follows the planar geometry of the host stratigraphy and is further defined by contact-parallel shear veins and horizontal to shallowly south-dipping quartz±ankerite extensional veins.

Crosscut CC300-152

Crosscut CC300-152 (Fig. 6b) preserves shear zones that are localized within chloritic siltstone, between tightly folded BIF intervals in the 1150 lodes. Quartz±ankerite shear veins are coincident with D_2B shear planes (Fig. 5d). Shallowly, south-dipping quartz±ankerite extensional veins, associated with shear zones, occur in both the BIF and siltstone units (Fig. 5e,f). These extensional veins are up to 50 cm thick in the BIF but generally less than 10 cm thick in the siltstone. The extensional veins are refracted in the BIF intervals, and are weakly to strongly deformed in the intensely foliated siltstone. Stratabound arsenopyrite±pyrrhotite replaces magnetite-rich layers within the BIF intervals where quartz±ankerite vein selvages are present (Fig. 5g). In contrast, this pattern of alteration in largely absent in the siltstone intervals.

Crosscut CC300-153

Crosscut CC300-153 (Fig. 6c), which is located approximately 15 m east of crosscut CC300-152, exposes tighter folds, relative to those present in crosscut CC300-152. The 1150 lodes are well developed in this area, with shear veins that follow F_2A fold limbs in BIF intervals and associated shallowly south-dipping extension veins with distinctive arsenopyrite replacement halos. The S_2A fabric is axial planar to F_2A folds and slightly steeper than the D_2B shear zones.

Crosscut CC325-155

Crosscut CC325-155 (Fig. 6d) exposes a weakly deformed, subvertical, ore-bearing quartz±ankerite vein with a weak sericite-alteration halo that cuts BIF. Stratabound arsenopyrite and minor pyrrhotite replacement of magnetite-rich layers within the BIF are associated with the selvages of this vein.

Geometry of the 1150 zone

Horizontal to shallowly south-dipping extensional veins and related shear zones and fault-fill veins are preferentially developed in tightly F_2A/F_2B folded decimetre to metre thick BIF layers on both sides of the moderately north-dipping reverse shear zones (Fig. 6b–d; St.Pierre et al., 2018, 2019). Further investigation of the oriented samples revealed that there are distinct shear bands cutting the main deposit fabric. Kinematic indicators within the late shear bands are consistent with dextral shear localized within the chloritic siltstone. This indicates that the main deformation and its

Figure 5 opposite page. a) Photograph of the Lower Fault, looking west. The fault is characterized by overprinting fabrics and lineations with a late gouge zone. **b)** East wall of crosscut CC200-167 showing the shear-hosted 1000 lode main vein and the associated mineralization, alteration halo, and sulphidation. Photograph courtesy of Agnico Eagle Mines Limited. **c)** The West wall of crosscut CC200-157 showing the "interveining lodes" immediately north of the 1000 lode. The interveining lodes are represented by multiple generations of progressively deformed extensional vein arrays that are hosted by Tiriganiaq Formation sedimentary rocks. The extensional veins are predominantly subhorizontal to shallowly north-dipping and are intensely transposed and folded. **d)** Representative structures associated with D_2B shear zones and associated extensional veins within the 1150 zone in crosscut CC300-152 (East wall). D_2B shear planes cut and drag a steeper S_2A fabric forming a localized shear zone along a highly strained limb of an F_2A-folded BIF layer. **e)** Coarse, idioblastic arsenopyrite replacement in BIF along a quartz±ankerite vein selvage. **f)** Photograph of the 1150 zone in crosscut CC300-152 (East wall) showing a series of shallowly south-dipping D_2B quartz-arsenopyrite±ankerite-pyrrhotite veins and bedding-parallel BIF replacement (1). Veins that extend into siltstone tend to contain much less sulphide (2). Veins that cut the weaker (?) and intensely foliated sedimentary rocks also tend to be refracted and transposed. In some cases, the BIF-hosted veins do not extend into chloritic siltstone bands. **g)** Schematic drawing of photograph (f) showing the host rocks (blue and dark grey), barren and mineralized veins (white and yellow, respectively), and the associated arsenopyrite-rich alteration halos (light grey). Abbreviations: Ank = ankerite, Apy = arsenopyrite, BIF = banded iron formation, Qtz = quartz.

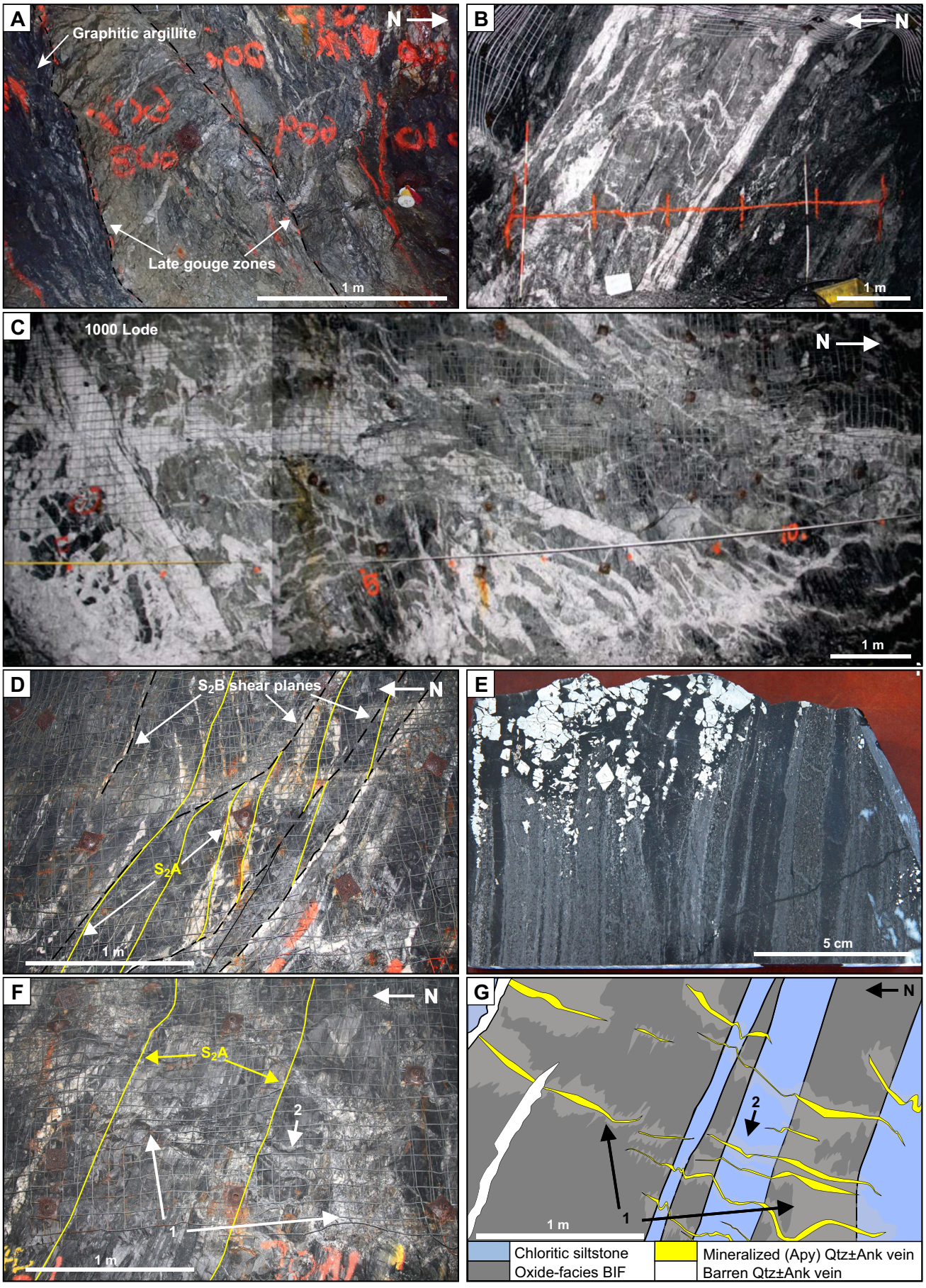
A
Graphitic argillite
Late gouge zones
1 m
N
B
1 m
N
C
1000 Lode
N
1 m
D
S_2B shear planes
S_2A
1 m
N
E
5 cm
F
S_2A
2
1
1 m
N
G
2
1
1 m
N
Chloritic siltstone
Oxide-facies BIF
Mineralized (Apy) Qtz±Ank vein
Barren Qtz±Ank vein

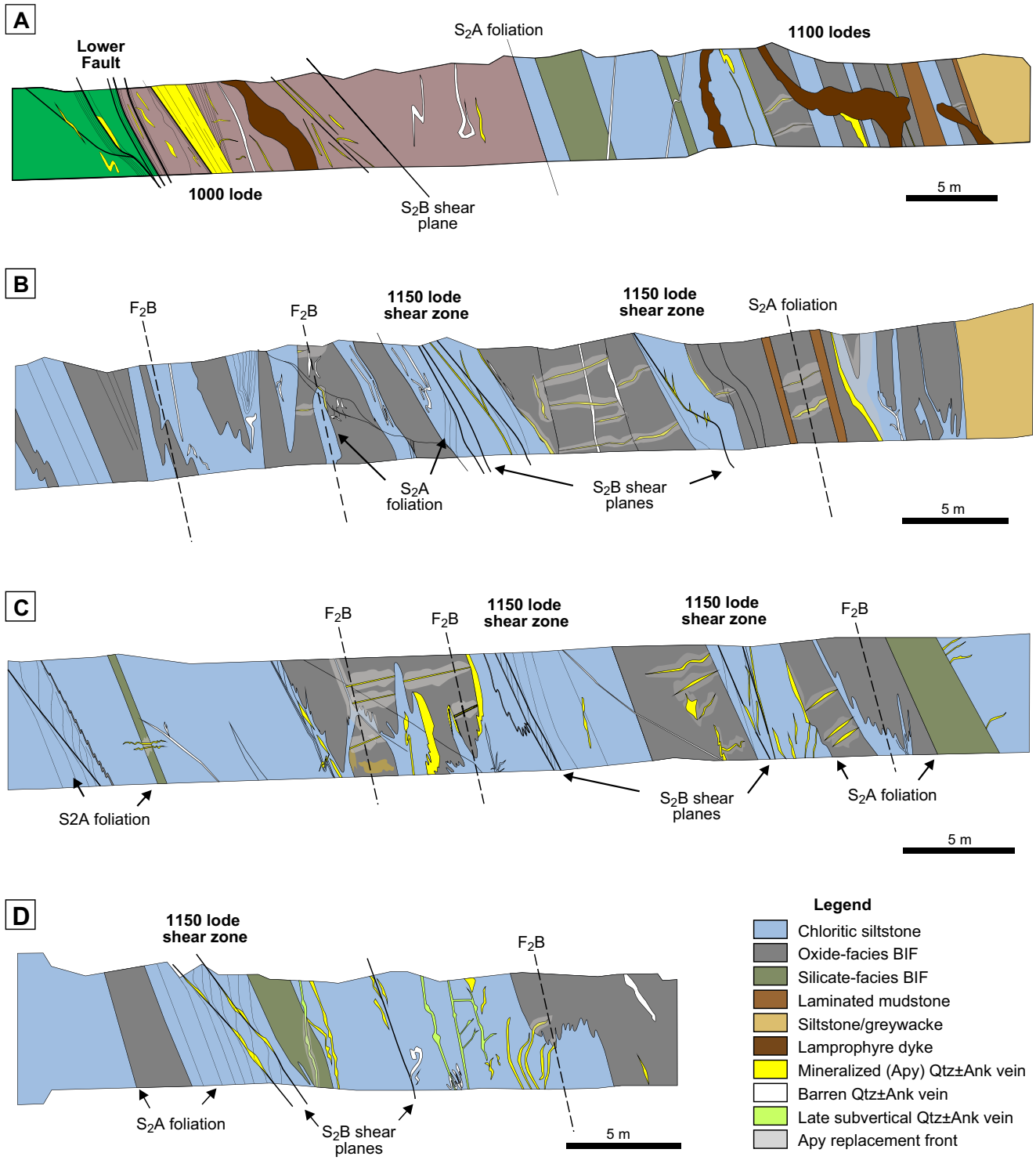

Figure 6. Detailed geological and structural maps of the underground workings of the 1000, 1100, and 1150 lodes at the Tiriganiaq deposit. **a)** The West wall of draw-point DP200-161 (level 200, 200 m below surface). The section exposes the Wesmeg Formation in the structural footwall of the Lower Fault, with the 1000 lode in the hanging wall of the fault. It also shows late lamprophyre dykes that cut across folded units. Further to the north is the 1150 lode corridor that consists of F_2A folded (long limbs exposed) and mineralized BIF units overprinted by moderately north-dipping S_2B shears. **b)** The West wall of crosscut CC300-152 (level 300, 300 m below surface). The section shows F_2A/F_2B folded BIF units (limbs and hinges are exposed) with narrow, weakly mineralized S_2B shear veins along the limbs and shallowly south-dipping extension veins. **c)** The West wall of stope CC300-153, 15 m east of crosscut CC300-152. The section displays well preserved F_2A/F_2B fold hinges and well developed S_2B shear-parallel veins with localized extension veins in the BIF units. **d)** The West wall of crosscut CC325-155 (level 325, 325 m below surface). The section shows weakly mineralized, narrow S_2B shear zones and a series of subvertical veins that are localized at the intersection with BIF units. Abbreviations: Ank = ankerite, Apy = arsenopyrite, BIF = banded iron formation, Qtz = quartz.

associated fabric have an oblique reverse dextral shear component, consistent with a major, syn-ore, reverse component of motion in the deposit area (St.Pierre et al., 2019).

In addition to the syn-D_2 ore-bearing shear veins and associated extensional veins, which are typical of the 1150 and 1250 lode series, there are also rare, relatively weakly deformed (transposed and boudinaged) subvertical quartz±ankerite veins (N270/88). Some of these veins carry gold where they intersect BIF and form stratabound replacement zones of coarse idioblastic arsenopyrite and minor pyrrhotite, which is typical of other BIF-hosted zones in the Upper Oxide Formation (Fig. 6d).

DISCUSSION

Relative Timing of Events

The best evidence for an early, pre-1900 Ma phase of deformation (D_1) comes from observed pre-F_2 mineral lineations, and stratigraphic and structural facing reversals within the upper volcanic cycle (Tella et al., 1986; Tella, 1994; Carpenter and Duke, 2004; Carpenter et al., 2005). However, Re-Os arsenopyrite model ages that range from 2270 to 1800 Ma provide evidence for a formerly unrecognized, pre-1860 Ma hydrothermal event(s) (Lawley et al., 2015b). Although these analyses may reflect isotopic disturbance and samples were gold-poor, there is still a possibility of an additional pre-1860 Ma hydrothermal event(s) (Lawley et al., 2015b). Deformed Paleoproterozoic conglomerate, which is folded with the Neoarchean stratigraphy, provided the most robust maximum age estimate for the main phase of deformation at ≤2155 Ma (Davis et al., 2008; Lawley et al., 2015b).

Gold mineralization at the Tiriganiaq deposit has previously been attributed to reworking and metamorphism during the Trans-Hudson Orogeny (1900–1800 Ma: Carpenter and Duke, 2004; Carpenter et al., 2005; Lawley et al., 2015a,b,c, 2016). This interpretation is favoured because D_2B mineralized reverse shear zones localized within chloritic siltstone contain mineralized quartz veins along S_2B shear planes that drag S_2A foliation. Also, associated horizontal to shallowly south-dipping mineralized extensional veins preferentially form within intercalated decimetre to metre wide F_2B-folded BIF. These and other observations, which are present at different scales, all agree with a major syn-ore incremental compressional deformation event (D_2). In this model, D_2 deformation starts with north-east-southwest shortening (D_2A) and a phase of layer-parallel F_2A isoclinal folding of the host successions and associated development of F_2A fold axial-planar and regionally penetrative S_2A cleavage. Thrusting and mineralized veining along the Pyke and Lower faults likely started at the onset of the D_2 deformation event (i.e. D_2A), as suggested in Miller et al. (1995). This was followed by, or transitioned to, a slight change in shortening orientation to north-south (D_2B) creating east-west regional asymmetric F_2B Z-folds and axial planar S_2B cleavage. The original boundary between the Chesterfield Block and Hearne Craton likely played a role in the timing and change in orientation of the developing penetrative fabrics (Berman et al., 2007). Progressive folding was associated with more brittle-ductile deformation (D_2B) until tightened folds could not accommodate further shortening. Preferential strain partitioning along fold hinges/limbs, relatively less competent units, and lithological contacts most likely led to the development of reverse shear zones. Ore-bearing shear veins were emplaced along shear planes that dragged the S_2A foliation. Mineralized localized shear zones and associated extensional veins were therefore emplaced during the D_2B deformation phase. The D_2C deformation consisted of S_2C crenulation cleavage development and associated kink-band development formed by continued shortening in the same orientation, which resulted in the emplacement of multiple generations of mineralized vein emplacement and progressive deformation. This is supported by variably deformed extensional vein arrays. However, this could also be explained by a mixture of fluid overpressure processes and/or changes in the strain rate, or temperature during deformation. Therefore, D_2 deformation can be constrained by the onset of the regional Trans-Hudsonian metamorphic event at ca. 1900–1850 Ma and by undeformed 1830 Ma lamprophyre dykes (Lawley et al., 2016).

Gold emplacement can be constrained further with U-Pb xenotime results that yield an upper intercept concordia age at 1862 ± 29 Ma on mineralized veins (Lawley et al., 2015b). This agrees with a $^{207}Pb/^{206}Pb$ monazite age of 1854 ± 6 Ma (Carpenter et al., 2005). Additionally, Re-Os dating suggest that ore-associated arsenopyrite-galena-ilmenite phases locally formed at ≥1860 Ma (Lawley et al., 2015a,b).

The D_3 deformation resulted in box folds within well foliated rocks along the Lower Fault zone, brittle fault gouges overprinting previous fabrics/structures, re-activation of the Lower Fault truncating post-D_2 deformation lamprophyre dykes, and subvertical relatively weakly deformed ore-bearing quartz±ankerite veins (N270/88) representing vertical compression and perhaps a phase of horizontal extension. Although considered a separate deformation event, the D_3 deformation could also represent the latest increment of the D_2 deformation. Ongoing work as part of this project should help resolve this question. The transition to brittle deformation and horizontal extension could hypothetically be linked with crustal relaxation after major compression, or it could be associated with the onset of

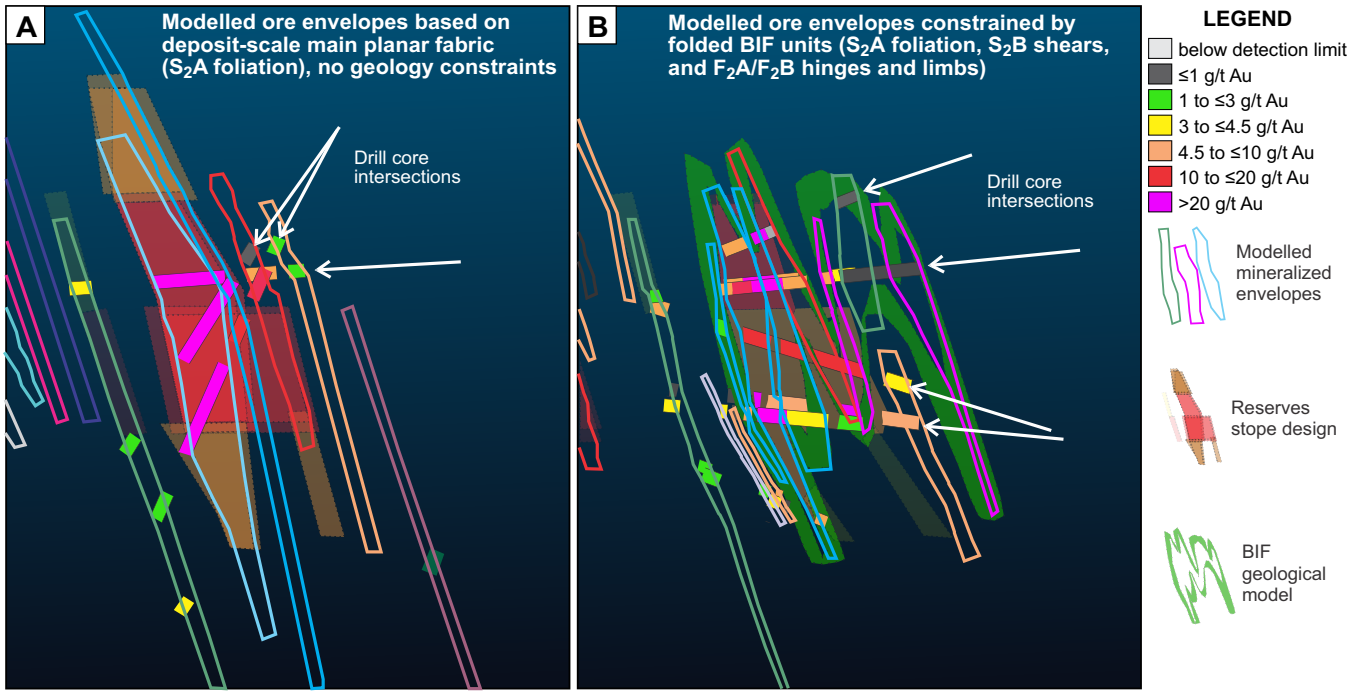

Figure 7. Sketch showing two models of the Tiriganiaq deposit, the first using knowledge before this study and the second using knowledge gained through this study. **a)** Modelling of typical ore zones based on drillhole intersections and the assumption that gold intersections are continuous and can be interpolated and extrapolated parallel to the main fabric. **b)** A revised model using information gained through this study and a better understanding of the combined structural and lithological controls on gold, which now integrates the folding and geometry of the BIF units and the presence of BIF-bound ore intervals, such as shallowly south-dipping extensional veins. Simplified from material provided by Agnico Eagle Mines Limited. Abbreviation: BIF = banded iron formation.

regional magmatism (e.g. Christopher Island Formation at 1830 Ma; Hudson granite suite at 1830 Ma; Nueltin granite suite at 1750 Ma; and the MacRae dyke swarm at 1750 Ma). Since D_3 deformation is associated with Lower Fault re-activation that truncates unfoliated lamprophyre dykes, it is likely that D_3 is younger than 1830 Ma. If regional magmatism played a role in deposit-scale horizontal extension and vertical compression, it would imply that D_3 could be constrained by the end of regional magmatism at ca. 1750 Ma and could potentially extend gold mineralization until ca. 1750 Ma. Further work planned at the Tiriganiaq deposit aims at clarifying the timing of events and should provide more insight into the timing and implications of the late deformation events.

IMPLICATIONS FOR MINE DEVELOPMENT AND EXPLORATION

New field relationships document the importance of horizontal to shallowly south-dipping ore-bearing D_2B/D_2C extensional quartz±ankerite veins. These veins and their associated sulphide replacement zones are preferentially developed in tightly F_2A/F_2B folded oxide-facies BIF intervals. The 1150 and 1250 lodes provide an excellent example of the type of geometric complexities of ore-bearing veins found within shallowly west-plunging F_2B folded BIF successions. These zones provide some of the highest gold grades and thickest gold intervals within the Tiriganiaq deposit and thus represent excellent exploration targets for both within the Tiriganiaq deposit as well as regionally within the RIGB. However, the orientation of these ore-bearing veins and their associated hydrothermal alteration zones were difficult to document in the absence of oriented drill core. Access to the 1150 lodes underground and their detailed documentation and study at drift scale as part of the current study helped understand the controls and geometry of these gold-rich zones.

This information significantly aided in stope design, 3-D modelling, and resource estimation. The revised understanding of the structural controls at play at the Tiriganiaq deposit that based on the results of this study provide excellent criteria for targeting near-mine and regional exploration by highlighting: 1) the importance of F_2A and F_2B fold hinge zones and their effect on the generation of favourable traps (thickened BIF intervals); and 2) the development of narrow shears along the limbs (S_2B) and the development of associated extensional veins in the BIF. Figure 7 illustrates how a better understanding of the geometry of the host BIF unit and the structural controls on the ore-bearing veins of the 1150 lodes could impact modelling results and grade and tonnage estimates. Updated modelling of

these ore zones now includes the folded geometry of the host BIF units (favourable host), the distribution of the veins along the sheared limbs (shear veins), and the development of shallowly dipping mineralized veins within the hinge zones of thickened BIF layers.

ONGOING AND FUTURE WORK

Results presented here are part of an ongoing M.Sc. research project, and current and future work includes analysis of the larger scale geometry of the ore zones and high-grade gold intercepts in 3-D. Whole rock geochemical analyses of the host rocks and mineralized zones will be applied to identify reliable stratigraphic markers within the complexly deformed stratigraphy and to define potential lithological control(s) on gold grade. Project results aim to improve stope design, reserve modelling, and exploration models by providing key information about the structural controls (conduits and traps) influencing the ore zones at various scales.

ACKNOWLEDGMENTS

This report is a contribution to the Targeted Geoscience Initiative Program (TGI-5) of the Geological Survey of Canada. Support for this study was provided through activity G-2.4 of the Gold project. B. St.Pierre is conducting a TGI-supported M.Sc. study at Institut national de la Recherche scientifique, Centre Eau, Terre, Environnement, Québec. This activity is conducted in close collaboration with the Meliadine Division and Technical Services divisions of Agnico Eagle Mines Limited that provided essential scientific and technical support as well as access to material and data. We are particularly grateful to M. Hjorth and G. Dyck from the Meliadine Division, and to B. Dubé and W. Bleeker for fruitful discussions of the geology of orogenic gold districts. Thanks to K. Lauzière and F. Aucoin for their help with Figure 7. This report benefited from thorough reviews by B. Frieman and C. Lawley. We also acknowledge E. Ambrose and V. Bécu for their editorial handling and review.

REFERENCES

Agnico Eagle Mines Limited, 2019. Agnico Eagle Mines Limited Detailed Mineral Reserves and Resources Data: As of December 31, 2017; Agnico Eagle Mines Limited. <https://www.agnico eagle.com/English/operations and development projects/ reserves and resources/default.aspx> [accessed January 23, 2019]

Bannatyne, M.J., 1958. The geology of the Rankin Inlet area and North Rankin Nickel Mines Limited, Northwest Territories; M.Sc. thesis, University of Manitoba, Winnipeg, Manitoba, 83 p.

Barham, B., 2010. Geological map of the Meliadine gold property, interpretation and compilation – Nov. 2009; Comaplex Minerals Corp. internal report.

Bell, C., 2013. Structural controls on gold mineralization at the Homestake mine and their implications for the geology of the Black Hills; Ph.D. thesis, James Cook University, Townsville, Queensland, Australia, 232 p.

Berman, R.G., Davis, W.J., Ryan, J.J., and Brown, N., 2002. In situ SHRIMP U-Pb geochronology of Barrovian facies-series metasedimentary rocks in the Happy Lake and Josephine River supracrustal belts: implications for the Paleoproterozoic architecture of the northern Hearne Domain, Nunavut; Geological Survey of Canada, Current Research 2002-F4, 14 p.

Berman, R., Davis, W., and Pehrsson, S., 2007. Collisional Snowbird tectonic zone resurrected: Growth of Laurentia during the 1.9 Ga accretionary phase of the Hudsonian orogeny; Geology, v. 35, p. 911–914.

Carpenter, R.L. and Duke, N.A., 2004. Geological setting of the West Meliadine gold deposits, Western Churchill Province, Nunavut, Canada; Exploration and Mining Geology Journal, v. 13, p. 49–65.

Carpenter, R.L., Duke, N.A., Sandeman, H.S., and Stern, R., 2005. Relative and absolute timing of gold mineralization along the Meliadine trend, Nunavut, Canada: evidence for Paleoproterozoic gold hosted in an Archean greenstone belt; Economic Geology, v. 100, p. 567−576.

Davis, W.J., Ryan, J.J., Sandeman, H.A., and Tella, S., 2008. A Paleoproterozoic detrital zircon age for a key conglomeratic horizon within the Rankin Inlet area, Kivalliq region, Nunavut: Implications for Archean and Proterozoic evolution of the area; Geological Survey of Canada, Current Research 2008-08, 8 p.

Dubé, B., Mercier Langevin, P., Castonguay, S., McNicoll, V.J., Bleeker, W., Lawley, C.J.M., De Souza, S., Jackson, S.E., Dupuis, C., Gao, J. F., Bécu, V., Pilote, P., Goutier, J., Beakhouse, G.P., Yergeau, D., Oswald, W., Janvier, V., Fontaine, A., Pelletier, M., Beauchamp, A. M., Katz, L.R., Kontak, D.J., Tóth, Z., Lafrance, B., Gourcerol, B., Thurston, P.C., Creaser, R.A., Enkin, R.J., El Goumi, N., Grunsky, E.C., Schneider, D.A., Kelly, C.J., and Lauzière, K., 2015. Precambrian lode gold deposits — a summary of TGI 4 contributions to the understanding of lode gold deposits, with an emphasis on implications for exploration; *in* Targeted Geoscience Initiative 4: Contributions to the understanding of Precambrian lode gold deposits and implications for exploration, (ed.) B. Dubé and P. Mercier Langevin; Geological Survey of Canada, Open File 7852, p. 1–24.

Goldfarb, R., Baker, T., Dubé, B., Groves, D., Hart, C., and Gosselin, P., 2005. Distribution, character and genesis of gold deposits in metamorphic terranes; *in* Economic Geology 100th Anniversary Volume, (ed.) J.W. Hedenquist, J.R.H. Thompson, R.J. Goldfarb, and J.P. Richards; Society of Economic Geologists, p. 407–450.

Lawley, C.J.M., Dubé, B., Mercier Langevin, P., McNicoll, V.J., Creaser, R.A., Pehrsson, S., Castonguay, S., Blais, J.-C., Simard, M., Davis, W.J., and Jackson, S.E., 2015a. Setting, age, and hydrothermal footprint of the emerging Meliadine gold district, Nunavut; *in* Targeted Geoscience Initiative 4: Contributions to the understanding of Precambrian lode gold deposits and implications for exploration, (ed.) B. Dubé and P. Mercier Langevin; Geological Survey of Canada, Open File 7852, p. 99–111.

Lawley, C.J.M., Creaser, R.A., Jackson, S., Yang, Z., Davis, B., Pehrsson, S., Dubé, B., Mercier Langevin, P., and Vaillancourt, D., 2015b. Unravelling the Western Churchill Province Paleoproterozoic gold metallotect: Constraints from Re-Os arsenopyrite and U-Pb xenotime geochronology and LA-ICP-MS arsenopyrite trace element chemistry at the BIF-hosted Meliadine gold district, Nunavut, Canada; Economic Geology, v. 110, p. 1425–1454.

Lawley, C.J.M., Dubé, B., Mercier Langevin, P., Kjarsgaard, B.A, Knight, R., and Vaillancourt, D., 2015c. Defining and mapping hydrothermal footprints at the BIF-hosted Meliadine gold district, Nunavut, Canada; Journal of Geochemical Exploration, v. 155, p. 33–55.

Lawley, C.J.M., McNicoll, V.J., Sandeman, H., Pehrsson, S., Simard, M., Castonguay, S., Mercier Langevin, P., and Dubé, B., 2016. Age and geological setting of the Rankin Inlet greenstone belt and its relationship to the gold endowment of the Meliadine gold district, Nunavut, Canada; Precambrian Research, v. 275, p. 471–795.

MacLachlan, K., Davis, W.J., and Relf, C., 2005. Paleoproterozoic reworking of an Archean thrust fault in the Hearne Domain, Western Churchill Province: U-Pb geochronological constraints; Canadian Journal of Earth Science, v. 42, p. 1313–1330.

Miller, A.R., Balog, M.J., and Tella, S., 1995. Oxide iron formation hosted lode gold, Meliadine Trend, Rankin Inlet Group, Churchill Province, Northwest Territories; Geological Survey of Canada, Current Research 1995-C, p. 163–174.

Pehrsson, S., Berman, R., and Davis, W., 2013. Paleoproterozoic orogenesis during Nuna aggregation: A case study of reworking of the Rae craton, Woodburn Lake, Nunavut; Precambrian Research, v. 232, p. 167–188.

Phillips, G.N., Groves, D.I., and Martyn, J.E., 1984. An epigenetic origin for Archean banded iron-formation-hosted gold deposits; Economic Geology, v. 79, p. 162–171.

Robert, F., Poulsen, K.H., and Dubé, B., 1994. Structural analysis of lode gold deposits in deformed terranes; Geological Survey of Canada, Open File 2850, p. 5–17.

St.Pierre, B., Mercier Langevin, P., Simard, M., Côté Mantha, O., Malo, M., and Servelle, G., 2018. Structural and lithologic controls on the nature and distribution of gold in the BIF associated 1150 and 1250 lode series at Tiriganiaq, Meliadine district, Rankin Inlet greenstone belt, Nunavut; *in* Targeted Geoscience Initiative: 2017 report of activities, volume 1, (ed.) N. Rogers; Geological Survey of Canada, Open File 8358, p. 157–161.

St.Pierre, B., Mercier Langevin, P., Simard, M., Côté Mantha, O., Malo, M., and Servelle, G., 2019. Structural and lithological controls on the nature and distribution of gold at the Tiriganiaq deposit, Meliadine district, Rankin Inlet greenstone belt, Nunavut; *in* Targeted Geoscience Initiative: 2018 report of activities, volume 1, (ed.) N. Rogers; Geological Survey of Canada, Open File 8549, p. 77–82.

Tella, S., 1994. Geology, Rankin Inlet (55K/16), Falstaff Island (55J/13) and Quartzite Island (55J/11), district of Keewatin, Northwest Territories; Geological Survey of Canada, Open File 2968, 2 sheets, 1 CD-ROM.

Tella, S., Annesley, I.R., Borradaile, G.J., and Henderson, J.R., 1986. Precambrian geology of parts of Tavani, Marble Island, and Chesterfield Inlet map areas, district of Keewatin: A progress report; Geological Survey of Canada, Paper 86-13, 20 p.

Tella, S., Mikkel, S., Armitage, A.E., Seemayer, B.E., and Lemkow, D., 1992. Precambrian geology and economic potential of the Meliadine Lake-Barbour Bay region, district of Keewatin, Northwest Territories; *in* Current Research, Part C; Geological Survey of Canada, Paper 92-1C, p. 1–11.

Tella, S., Roddick, J.C., and van Breemen, O., 1996. U-Pb zircon age for a volcanic suite in the Rankin Inlet Group, Rankin Inlet map area, district of Keewatin, Northwest Territories; *in* Radiogenic Age and Isotopic Studies, Report 9; Geological Survey of Canada, Current Research 1995-F, p. 11–15.

Vial, D.S., deWitt, E., Lobato, L.M., and Thorman, C.H., 2007. The geology of the Morro Velho gold deposit in the Archean Rio das Velhas greenstone belt, Quadrilátero Ferrífero, Brazil; Ore Geology Reviews, v. 32, p. 511–542.